

# The Palomar Abell Cluster Optical Survey I: Photometric Redshifts for 431 Abell Clusters

R.R. Gal<sup>1</sup>, R.R. de Carvalho<sup>2</sup>, R. Brunner, S.C. Odewahn<sup>3</sup> & S.G. Djorgovski

*Palomar Observatory, Caltech, MC105-24, Pasadena, CA 91125*

## ABSTRACT

This paper presents photometric redshifts for 431 Abell clusters imaged as part of the Palomar Abell Cluster Optical Survey (PACOS), of which 236 are new redshifts. We have obtained moderately deep, 3-band (Gunn *gri*) imaging for this sample at the Palomar Observatory 60'' telescope, as part of the photometric calibration of DPOSS. Our data acquisition, reduction, and photometric calibration techniques are described, and photometric accuracy and consistency is demonstrated. An empirical redshift estimator is presented, utilizing background-corrected median  $g - r$  colors and mean  $g$  magnitudes for the ensemble of galaxies in each field. We present photometric redshift estimates for the clusters in our sample with an accuracy of  $\sigma_z = 0.038$ . These redshift estimates provide checks on single-galaxy cluster redshifts, as well as distance information for studies of the Butcher-Oemler effect, luminosity functions,  $M/L$  ratios, and many other projects.

*Subject headings:* catalogues – surveys – galaxies: clusters: general

## 1. Introduction

Clusters of galaxies are the largest bound systems in the Universe providing useful constraints for theories of large-scale structure formation and evolution. They are the samples of choice for studying galaxy evolution in dense environments, with many tens or even hundreds of galaxies in a small, physically associated volume. Multicolor optical photometry of galaxy clusters is commonly used to study the Butcher-Oemler effect (Butcher & Oemler 1978), the morphology-density relation (Dressler 1980), and other correlations between overall cluster properties, galaxy properties, and redshift. Comparisons between optical and X-ray properties of galaxy clusters are also of considerable scientific interest. For instance, mass-to-light ratios of clusters are also useful for constraining cosmological parameters, including  $\Omega$ , the mass density of the universe. Properly understood catalogs in the optical and X-ray can help us better understand the various selection effects present in both types of cluster samples.

To obtain the maximal scientific return from such studies, it is necessary to know the redshifts of the clusters. Unfortunately, the majority of known galaxy clusters do not have measured redshifts. Nearly fifty years has passed since the publication of Abell's (1958) optically selected cluster catalog, and only  $\sim 1/3$  of the Northern clusters have had spectroscopically measured redshifts, with many of these based on only one or two galaxies. Even at low redshift, obtaining accurate cluster redshifts requires a four-meter class

---

<sup>1</sup>Email: rrg@astro.caltech.edu

<sup>2</sup>Observatório Nacional, Rua Gal. José Cristino, 77 – 20921-400, Rio de Janeiro, RJ, Brazil

<sup>3</sup>Arizona State University, Dept. of Physics & Astronomy, Tempe, AZ 85287

telescope with multi-object spectroscopic capability; performing a survey of hundreds or even thousands of clusters is prohibitively time consuming.

In recent years, there has been an increasing recognition that redshifts of individual objects or clusters can be estimated quite accurately from photometric data (Frei & Gunn 1994, Brunner *et al.* 1997, *etc.*) These estimators have traditionally relied on either empirical correlations between individual galaxy colors and spectroscopically measured redshifts (Connolly *et al.* 1995), or a template method wherein model spectra are created from evolutionary synthesis codes or spectroscopic data (Gwyn & Hartwick 1996). However, both techniques aim to measure the redshifts of single objects using many ( $n \geq 4$ ) colors; increasing the number of colors results in more accurate redshifts over a larger redshift range. An extensive discussion and comparison of existing techniques can be found in Hogg *et al.* (1998). Unlike these methods, we are instead relying on only two filters (Gunn  $g$  and  $r$ ) to derive photometric redshifts for an ensemble of objects (a galaxy cluster) over a relatively small redshift range ( $0 < z < 0.3$ ). Prior methods for estimating cluster redshifts have generally relied on the magnitude of the  $n$ -th brightest galaxy (Abell 1958, Dalton *et al.* 1994).

Using a small (1-meter class) telescope, equipped with a large-format CCD, one can obtain photometric data on a very large sample of clusters. Greater amounts of observing time are more readily scheduled on such telescopes, and the integration times required for imaging are much shorter than for spectroscopy to comparable depths on larger telescopes. In addition, many optical imaging surveys, such as the Digitized Second Palomar Sky Survey (DPOSS, Djorgovski *et al.* 1999) and the Sloan Digital Sky Survey (SDSS, Gunn & Weinberg 1995), provide photometric data which can be used for this purpose. For instance, Gal *et al.* (2000) presented a simple photometric estimator for galaxy clusters found in DPOSS, and the SDSS photometric system (Fukugita *et al.* 1996) was designed specifically to improve photometric redshift estimation.

The success of these estimators spurred us to utilize our data on Abell clusters to measure their redshifts photometrically. We have observed 468 Abell clusters at the Palomar 60" telescope, using two different detectors, in the Gunn  $gri$  filters (Thuan & Gunn 1976, Wade *et al.* 1979). The primary purpose of these data are to provide precision photometric calibration for DPOSS. Nevertheless, this large, homogeneous dataset is a valuable resource in and of itself, and is ideal for photometric redshift estimation.

In the first section of this paper, we describe the telescope, CCD cameras, and data taking strategy used during the course of this survey. The second section describes the observing program. The third section presents our data reduction procedure and the derivation of photometric calibration, using Gunn standards which were imaged every night. We also demonstrate our photometric accuracy using data acquired on the same clusters on multiple nights and with different detectors. The fourth section presents the photometric redshift estimation technique, and our estimated redshift errors, as well as a table of the measured redshifts. We conclude with a brief discussion of our results.

## 2. Data Acquisition and Analysis

### 2.1. Telescope and Detectors

All data described in this paper were obtained at the Palomar Observatory 60" telescope. The telescope is an  $f/8.75$  Ritchey-Chretien design, with the CCD imaging cameras placed at Cassegrain focus. From the initial data through June 1996, and on rare occasions thereafter, we used CCD16, a SITE 1024<sup>2</sup>, thinned, AR coated array, with  $24\mu\text{m}$  pixels. The pixel scale is  $0.376''/\text{pixel}$ , providing a  $6.4' \times 6.4'$  field of view.

CCD16 has a gain of  $2.5e^-/DN$  and a read noise of  $8.2e^-$ . Starting in July 1996, a new, larger detector was made available at the Palomar 60". This detector, CCD13, is a SITe 2048<sup>2</sup> thinned, AR coated array, also with  $24\mu m$  pixels. The pixel scale at this detector is  $0.368''/\text{pixel}$ , providing a  $12.56' \times 12.56'$  FOV. CCD13 has a gain of  $1.63e^-/DN$  and a read noise of  $6.3e^-$ . In addition to the factor of four increase in area over CCD16, this detector also provides extremely good blue sensitivity ( $\sim 55\%$  *QED* at  $4000\text{\AA}$ ). All objects were observed in the Gunn *gri* filters.

## 2.2. Observations

The imaging targets are selected from the list of northern Abell Clusters (Abell, Corwin & Olowin 1989). Because the survey was designed to provide photometric calibration and star-galaxy separation data for DPOSS (Djorgovski *et al.* 1999), we attempted to observe at least two Abell clusters per DPOSS field (each field being  $\sim 36$  square degrees). Priority was given to the richest clusters closest to the plate centers; therefore, our sample is biased toward richer Abell clusters. Nevertheless, many plates have only one or two known clusters; in such cases, whatever clusters were available were observed. Approximately fifty clusters were observed twice, sometimes with both detectors. This allows us to check our photometric accuracy, as well as consistency between detectors.

Data were taken only on photometric nights with seeing better than  $2''$ . The mean seeing for our data is  $\sim 1.5''$ ; the best seeing is  $0.9''$ . Integration times were fixed for each filter/CCD combination, regardless of sky brightness or seeing. The vast majority of nights allocated for this program were  $> 75\%$  dark. For CCD16, we integrated for  $1200s$  in *g*, and  $900s$  each in *r* and *i*. When using CCD13, the integration times were shortened to  $900s$  in *g*, and  $600s$  each in *r* and *i*. These yielded limiting magnitudes of  $m_{lim,gri} \sim 22^m$  for CCD13 observations, with limiting magnitudes for CCD16 observations  $\sim 0.5$  magnitudes brighter. With the typical observational overhead, we usually observed between seven and eleven clusters in a single night.

For every night that was deemed photometric, we observed a set of Gunn standards. Between 5 and 12 observations of available Gunn standards were made each night, at a variety of airmasses. Each star observed at each pointing was observed three times on a single frame by closing the shutter, offsetting the telescope, and reopening the shutter. This was done to increase the S/N of our photometric measurements, as well as avoid excessive time loss due to the long ( $\sim 180s$ ) readout time for CCD13. In addition to the standard stars, we also took nine bias frames, nine dome flats in each filter, and three sky flats in each filter on every night of observing.

## 3. Data Processing

### 3.1. Image Reduction

Data were processed using the IRAF data reduction package (Tody 1986). First, a single bias value, determined from the median value in the overscan region of each image, was subtracted from all object and calibration frames. The bias frames were median filtered and fit with a smooth polynomial, which was subtracted from all object and flat field images. Individual dome and sky flats in each filter were median stacked, and the resulting sky flats processed with the dome flats. The remaining large scale structure was smoothed, and this smooth correction was recombined with the dome flats to create a master flat field image for each filter.

These master flat field corrections were applied to all target and standard star frames. After this procedure there were still noticeable large scale gradients in the CCD illumination pattern, especially in the  $g$  frames. To remove this, we generated dark sky flat field frames (also known as illumination corrections) by median filtering all of the unregistered target frames in each filter. On those nights where too few targets were observed to generate such an illumination correction, data were combined with an adjacent night. These combined images were smoothed with a large (50 pixel) boxcar, and the resulting correction applied to both the target and standard star frames. This procedure results in images that are flat to the  $\sim 1\%$  level. Finally, for CCD13, it was necessary to apply a fringe correction to the  $i$  images. This was generated by median stacking the completely flat-fielded  $i$ -band target images, and smoothing the result with a small (5 pixel) boxcar. The resulting image was used as the fringe correction for the target frames.

### 3.2. Photometric Calibration

Standard star photometry was performed using the *apphot* package in IRAF. Stars were photometered in numerous apertures up to 50 pixels (18.5") in radius, and the local sky was determined using a 10 pixel wide annulus centered on each star, starting at a radius of 50 pixels. The convergence magnitudes for all three exposures of each star on each frame were measured, and the three values averaged to provide a mean instrumental magnitude.

The resulting collection of between five and twelve measured instrumental magnitudes were used to determine the zero-point offset, airmass term, and color term in each filter. We used the IRAF *fitparams* task to fit the relation

$$m_{true} = m_{inst} + A + Bsec(z) + C(color) \quad (1)$$

for each filter. On some nights, not enough standards were observed to robustly determine values for all three unknowns. In these cases, the airmass and color terms were fixed at those derived from the mean values from nights with sufficient standards (given in Table 1), and only the zero point was determined. Typical *rms* deviations in the fit of the calibration relation are 0.01 magnitude. In addition, on two nights, over twenty Gunn standards were observed to test our measurements of the airmass and color terms. In both cases, the derived terms were within 10% of the mean values derived from other nights with many fewer standards.

### 3.3. Object Detection and Photometry

Object detection on the target frames was done using the FOCAS package (Jarvis & Tyson 1979, Valdes 1982). The  $g$ ,  $r$ , and  $i$  frames were processed independently, using detection parameters of  $2.5\sigma$  per pixel,

Table 1. CCD13 Extinction and Color Terms

Filter	Airmass	Color
$g$	-0.152	$0.150 \times (g - r)$
$r$	-0.094	$0.068 \times (g - r)$
$i$	-0.070	$-0.013 \times (g - i)$

a 25 pixel minimum area, and a sky value estimated individually for each image. Object classification was also performed by FOCAS, and the classifications were visually inspected. Bright objects with incorrect classifications (usually due to saturated pixels) were corrected by hand. The photometric coefficients derived from the standard star observations were used to determine object magnitudes. The color terms were applied only after objects are detected in multiple filters, and matched together at a later stage. For objects detected in only one filter, default colors of  $g-r = 0.5$  and  $g-i = 0.5$  were used when applying the color correction. In order to properly study such a large collection of imaging data, we must establish photometric consistency between many observing nights, and in our case, two different detectors. Photometric accuracy is also a necessary condition for using this data to calibrate DPOSS. To examine this question, we observed 51 clusters on two or more occasions. In some cases, both sets of observations were taken with the same CCD, and in others, with both CCDs.

We have compared the photometry of numerous, multiply-observed clusters in three scenarios: (1) both observations with CCD16, (2) one observation with CCD16 and one with CCD13, and (3) both observations with CCD13. We find that there are no systematic night-to-night or CCD-to-CCD photometric offsets greater than  $0.05^m$ , and the residuals are typically  $0.05^m$  at  $m_{gri} = 19^m$ , rising to no more than  $0.15^m$  for objects within one magnitude of the detection limit. Table 2 presents the typical residuals at  $m_r = 20.0^m$  for the various comparisons, while Figure 1 shows a typical set of photometric comparisons. The left plot is a comparison of photometry for the cluster A31, where both nights of data were taken with CCD16. The data were taken 14 months apart. The center plot compares photometry for the cluster A98, with one night of CCD16 data, and one night of CCD13 data. In this case, the data were taken almost four years apart. Finally, the right plot shows photometry for A2562, with both nights of data taken with CCD13, taken only 3 months apart. The bottom panels show the magnitude differences between each pair of observations.

#### 4. Photometric Redshifts

From the CCD data, we wish to measure the redshift of each cluster. This can be done either by estimating the redshift of each galaxy individually, and examining the resulting redshift distribution, or by using the properties of all the galaxies in the image. We have chosen to use the second method, for a number of reasons. First, we only have limited wavelength coverage. Having only three filters (and especially the lack of  $u$  images), makes it difficult to disentangle color-redshift degeneracies. Second, our photometric errors on individual objects are significant enough to pose a problem for an object-by-object redshift estimator. Finally, since we have performed object detection in the different filters independently (i.e. we do not have matched apertures), there may be systematic effects in the relative colors of different galaxy types. We have therefore elected to use the average properties of the galaxies in each field. Spectroscopic redshifts are taken

Table 2. Photometric Residuals at  $m_r = 20.0^m$

Comparison	$\sigma_g$	$\sigma_r$	$\sigma_i$
CCD16 <i>vs.</i> CCD16	0.19	0.13	0.09
CCD13 <i>vs.</i> CCD16	0.10	0.09	0.10
CCD13 <i>vs.</i> CCD13	0.12	0.10	0.16

from Struble & Rood (1991,1999).

#### 4.1. Deriving the Relation

We estimate the redshift assuming that each field contains a single cluster, at one redshift, and the cluster galaxy population is dominated by early-type galaxies. The  $g - r$  color of elliptical galaxies evolves rapidly at  $z < 0.4$  due to a strong  $k$ -correction, as the  $4000\text{\AA}$  break passes through the  $g$  filter. Similarly, the  $g$  magnitudes of these galaxies fade rapidly with redshift, due to both distance and  $k$ -correction effects. For these reasons, we have chosen to use the  $g - r$  colors and  $g$  magnitudes of the cluster galaxies in our photometric redshift estimator. The assumption of a single cluster per CCD field is reasonable, although projections are certain to occur. While it has been estimated that up to 35% of clusters in the Abell catalog with  $R \geq 1$  may be the result of projections of poorer clusters (van Kaarlem, Frenk & White 1997), our results will be dominated by the richest cluster in each field. Our redshift estimator will fail if there are two similarly rich clusters projected along the line of sight.

We count the number of galaxies as a function of color,  $N_{g-r}$ , and the number as a function of  $g$  aperture magnitude (where our aperture has a radius of 13 pixels, or  $\sim 5''$ ),  $N_g$ , inside each CCD frame, imposing a magnitude limit of  $m_r = 21.5^m$  for CCD 13 and  $m_r = 21.0^m$  for CCD16, to avoid incompleteness. We use the whole CCD area (as opposed to a given physical radius), because the size of our field is comparable to the sizes of clusters in the redshift range we are examining, and the centers of many clusters are not well determined.

First, we apply an extinction correction to the magnitudes and colors of all objects in our fields, derived from the maps of Schlegel *et al.* (1998). A single correction is used for each CCD field, since the pixel size of the extinction maps is comparable to the CCD FOV, and the vast majority of our fields are at high galactic latitudes; the mean  $E(B - V)$  for our sample is  $0.075^m$ . A statistical background correction must then be applied to both galaxy color and magnitude distributions. These corrections,  $N_{bg,g-r}$  and  $N_{bg,g}$  are determined from a set of 22 observations of random fields taken with CCD13, during numerous observing runs. This distribution (scaled to the appropriate area for CCD16 data), is then subtracted from the color and magnitude distributions of each cluster, and the median  $g - r$  color and mean  $g$  magnitude of the remaining galaxies calculated. An example showing this procedure is shown in Figure 2. The thin solid line is the distribution of all galaxy colors ( $g - r$ ) in CCD13 images of Abell 2063. The dotted line is the distribution of galaxy colors derived from our random field observations, while the thick solid line is the background-corrected distribution. A sharp peak at  $(g - r) \sim 0.5$  is seen, corresponding to the early-type galaxy population in this cluster.

Empirical relations between our measured cluster properties and the spectroscopic redshifts were then derived independently for CCD13 and CCD16 data. For CCD13, 114 clusters with measured redshifts were used, while only 33 clusters were available for CCD16. Using the GAUSSFIT package (Jefferys *et al.* 1988), we performed a bivariate least-squares fit, deriving the following relations between redshift, median  $g - r$  color, and mean  $g$  magnitude:

**CCD13, with  $m_{r,lim} = 21.5$ :**

$$\log(z) = 3.2619 \times (g - r)_{med} - 1.6687 \times (g - r)_{med}^2 + 0.1190 \times g_{mean} - 4.6532 \quad (2)$$

**CCD16, with  $m_{r,lim} = 21.0$ :**

$$\log(z) = 3.2151 \times (g - r)_{med} - 1.6957 \times (g - r)_{med}^2 + 0.0710 \times g_{mean} - 3.5983 \quad (3)$$

The formal errors on each coefficient from the fit are very small ( $\pm 0.0002$  or less). The above relations, although apparently dissimilar, should be universal, since we are using calibrated quantities. To test this, we applied the same magnitude cut ( $m_r < 21.0$ ) used for the CCD16 data to the CCD13 data. The coefficients from the CCD16 fit were then used to estimate redshifts for the CCD13 clusters with spectroscopic redshifts. The *rms* of  $z_{spect} - z_{phot}$  was only marginally higher (0.025 vs. 0.024) than using the true CCD13 fit, although a slight systematic overestimate of the redshift does occur at  $z < 0.1$ . The effects of detector area, the background correction technique, and the sample used can all affect the fit; nevertheless, it appears that our derived relations should be applicable to other data sets treated in an identical fashion (*i.e.* same filters, apertures, magnitude cuts, and background correction).

It is important to note that the combination of both color and magnitude information significantly improves our photometric redshift estimates. Figure 3 shows the photometric redshift estimates using magnitudes only, colors only, and the combination of colors and magnitudes for the CCD13 data. The scatter in redshift decreases from 0.034 for magnitudes only, to 0.031 for colors only, to 0.024 when both are used.

#### 4.2. Redshift Errors

The *rms* of  $z_{spect} - z_{phot}$  are  $\sigma(z) = 0.024$  and  $0.027$  for CCD13 and CCD16, respectively. These figures represent the intrinsic scatter of our derived relationship between redshift and photometric properties. The scatter is larger for the CCD16 data due to the small number of clusters with spectroscopic redshifts used in the derivation. The error on any individual cluster redshift depends not only on the scatter of the relation, but also on the number of clusters in the local redshift range used to determine the relation. For instance, at the high redshift end ( $z \sim 0.3$ ), there are only four clusters which constrain the relation for the CCD13 data. Therefore, we expect the errors in this redshift range to be larger than at  $0.05 < z < 0.1$ , where there are 29 clusters.

To estimate the magnitude of this effect, we have performed bootstrap simulations of our training samples. We randomly select clusters from our training sample, with replacement, until we have built a new training sample of the same size as the original (114 for CCD13, 33 for CCD16). This new sample is used to derive a new redshift estimator, which is then applied to the original sample. We repeat this procedure 500 times, and calculate the mean redshift estimate, and the standard deviations about this estimate, for each cluster. Figure 4 shows the photometrically estimated redshift against the spectroscopically measured redshift for both CCDs. Error bars on individual redshifts represent the one-sigma redshift limits from the bootstrap procedure.

Clearly, the errors are smallest in the redshift bins with the largest number of calibrating clusters. Figure 5 shows the errors on each cluster redshift derived from the bootstrap procedure. Solid circles show the mean redshift errors in bins of  $\Delta z = 0.05$ . For CCD13, the errors are largest at  $z \sim 0.3$ , where there are only 3 clusters. The redshift distribution for CCD16 clusters is more even, yielding nearly equal errors over the entire redshift range. To estimate the true redshift error on any given measurement, we add in quadrature the intrinsic scatter of our  $z_{phot}$  vs.  $z_{spec}$  relation, and the error from the appropriate bin from our bootstrap simulation. This error estimate then encompasses both the intrinsic errors of our fit, and the errors introduced from our sample selection. For 57 clusters, we have multiple observations from which to estimate their redshifts. Comparing these redshift estimates, we find *rms*  $\Delta z = 0.038$ , which is exactly what we expect from the individual error estimates. Our redshift errors are not dominated by photometric errors, since a large number of galaxies contribute to the mean color and magnitude values in each cluster. The scatter is most

likely due to inaccurate spectroscopic redshifts (less than 20% of the clusters have three or more galaxies with measured redshifts) and variance in the cluster properties (blue galaxy fraction, richness, *etc.* For instance, Miller *et al.* (1999) have demonstrated that projection effects have resulted in significantly erroneous redshifts for 14% of clusters with single spectroscopic redshifts. These two effects cannot be disentangled without a larger sample of clusters with properly measured spectroscopic redshifts. Unfortunately, almost all of the clusters we studied that also have a significant number of spectroscopic redshifts are very nearby ( $z < 0.05$ ), and therefore we cannot draw any significant conclusions about spectroscopic redshift errors for our sample as a whole.

W

e present the photometric results in Table 3. Clusters are arranged in numerical order. The first column gives the Abell cluster number. The second column gives the CCD used for the observation. The next two columns provide the background-corrected median ( $g - r$ ) color and  $g$  magnitude for each cluster. The fifth column is the extinction  $E(B - V)$ . The sixth column provides the photometric redshift estimate, and the seventh column contains the estimated error, as described above. The final column gives the spectroscopic redshift, if it is available. For clusters with very low spectroscopic redshifts ( $z_{spec} < 0.03$ ), we usually obtain a significantly higher photometric redshift. For these clusters, our CCD field covers only a small physical area, and we are likely seeing through the lower redshift cluster and measuring a background cluster.

## 5. Discussion and Future Work

This paper presents the data acquisition, reduction, and photometric analysis of an unprecedented sample of CCD *gri* observations of Abell clusters. We have demonstrated the photometric consistency of our sample, and presented a simple yet effective photometric redshift estimator. A total of 431 clusters have been studied, providing 236 new photometric redshift estimates. In addition, we have shown our photometric redshift estimator to be universal. The derived relations between redshift, colors, and magnitudes can be applied to any other data set taken with the same filters and analyzed in an identical way.

These new redshifts enable a variety of projects for which photometry alone is not sufficient, and distance information is required, but high accuracy is not necessary. The evolution of galaxy and cluster properties with time (i.e. the Butcher-Oemler effect, morphology-density relation, luminosity functions, *etc.*) are prime examples of such science. In addition, these photometric redshifts are a useful check on the spectroscopic redshifts of galaxy clusters, many of which are derived from a single measured galaxy.

Future papers will make use of this large sample to perform large, statistical studies of low redshift ( $z < 0.3$ ) galaxy clusters. The next paper will discuss the Butcher-Oemler effect (as was done for a smaller sample by Margoniner & de Carvalho 2000), and later papers will measure luminosity functions, study intracluster light, the color-magnitude relation, the Binggeli effect (Binggeli 1982), and galaxy morphology. Bringing in data from other wavelengths, most notably X-ray and radio, we will examine cluster  $M/L$  ratios, morphologies, cooling flows, the cluster fundamental plane, and radio properties of elliptical galaxies. Each paper will focus on a specific study of this vast statistical sample. Finally, the entire CCD data set (images as well as catalogs) will be released to the astronomical community.

RRG was supported in part by an NSF Fellowship, NASA GSRP NGT5-50215, and a Kingsley Fellowship. We thank the Norris Foundation for their generous support of the DPOSS project. We also thank the Palomar TAC and Directors for generous time allocations for the DPOSS calibration effort. Numerous past



and present Caltech undergraduates (V. Desai, V. Hradecky, J. Meltzer, B. Stalder, J. Hagab, R. Stob, J. Kollmeier) assisted in the taking of the data utilized in this paper.

## REFERENCES

- Abell, G. O. 1958, ApJS 3, 211
- Abell, G. O., Corwin, H. G. & Olowin, R. P. 1989, ApJS 70, 1
- Binggeli, B. 1982, A&A 107, 338
- Brunner, R. J., Connolly, A. J., Szalay, A. S. & Bershad, M. A. 1997, ApJ 482, L21
- Butcher, H. & Oemler, A., Jr. 1978, ApJ 226, 559
- Connolly, A. J., Csabai, I., Szalay, A. S., Koo, D. C., Kron, R. C., & Munn, J. A. 1995, AJ 110, 2655
- Dalton, G. B., Efstathiou, G., Maddox, S. J. & Sutherland, W. J., 1994, MNRAS 269, 151
- Djorgovski, S. G., Gal, R. R., Odewahn, S. C., de Carvalho, R. R., Brunner, R., Longo, G. & Scaramella, R. 1999, in *Wide Field Surveys in Cosmology*, S. Colombi *et al.*, eds., p. 89, (Paris: Editions Frontieres)
- Dressler, A. 1980, ApJ 236, 351
- Frei, Z. & Gunn, J.E. 1994, AJ 108, 1476
- Fukugita, M., Ichikawa, T., Gunn, J. E., Doi, M., Shimasaku, K. & Schneider, D. P. 1996, AJ 111, 4
- Gal, R. R., de Carvalho, R. R., Odewahn, S. C., Djorgovski, S. G. & Margoniner, V. E. 2000, AJ 119, 12
- Gunn, J. E. & Weinberg, D. H. 1995, in *Wide Field Spectroscopy and the Distant Universe* eds. S. Maddox & Aragon-Salamanca (World Scientific, Singapore), 3
- Gwyn, S. D. J., & Hartwick, F. D. A. 1996, ApJ 468, L77
- Hogg, D. W., Cohen, J. G., Blandford, R., Gwyn, S. J. *et al.* 1998, AJ 115, 1418
- Jarvis, J. F. & Tyson, J. A. 1979, Proc. SPIE 172, 422
- Jefferys, W. H., Fitzpatrick, M. J. & McArthur, B. E. 1998, Celestial Mechanics 41, 39
- Margoniner, V. E. & de Carvalho, R. R. 2000, AJ 119, 1562
- Miller, C. J., Batuski, D. J., Slinglend, K. A. & Hill, J.M. 1999, ApJ 523, 492
- Schlegel, D. J., Finkbeiner, D. P. & Davis, M. 1998, ApJ 500, 525
- Struble, M. F. & Rood, H. J. 1991, ApJS 77, 363
- Struble, M. F. & Rood, H. J. 1999, ApJS 125, 35
- Thuan, T. X. & Gunn, J. E. 1976, PASP 88, 543
- Tody D. 1986, SPIE 627, 733
- Valdes, F. 1982, Proc. SPIE 331, 465
- van Haarlem, M. P., Frenk, C. S. & White, S. D. M. 1997, MNRAS 287, 817
- Wade, R. A., Hoessel, J. G., Elias, J. H. & Huchra, J. P. 1979, PASP 91, 35

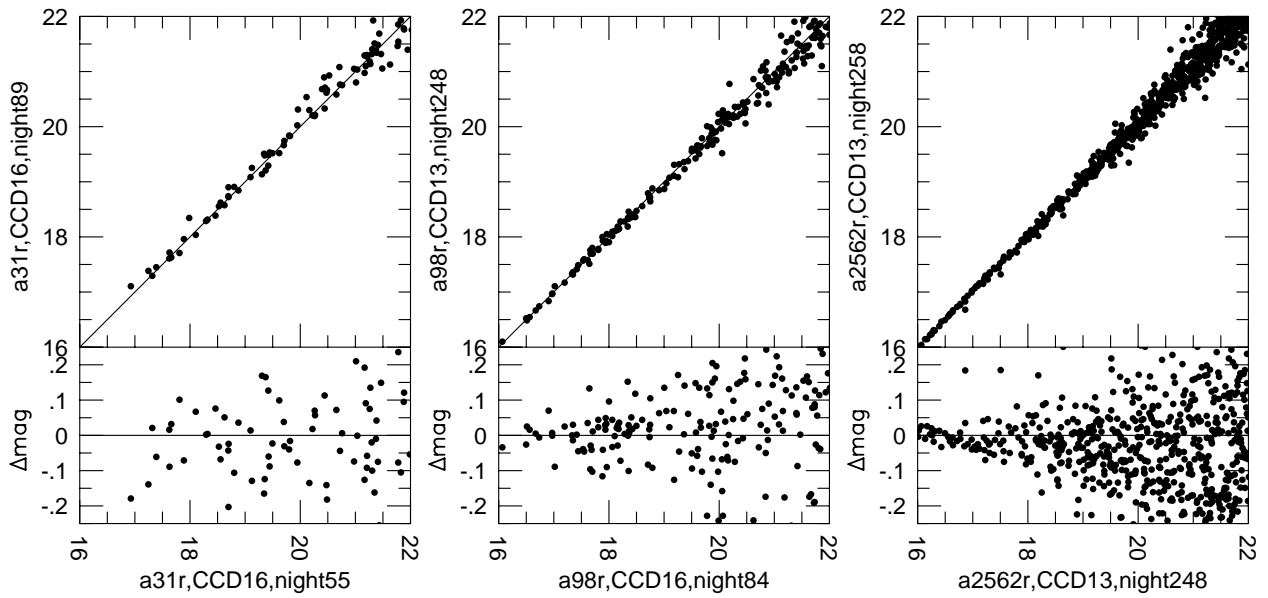


Fig. 1.— Typical photometric comparisons. The left plot is a comparison of photometry for the cluster A31, where both nights of data were taken with CCD16. The center plot compares photometry for the cluster A98, with one night of CCD16 data, and one night of CCD13 data. Finally, the right plot shows photometry for A2562, with both nights of data taken with CCD13. The bottom panels show the magnitude differences between each pair of observations.

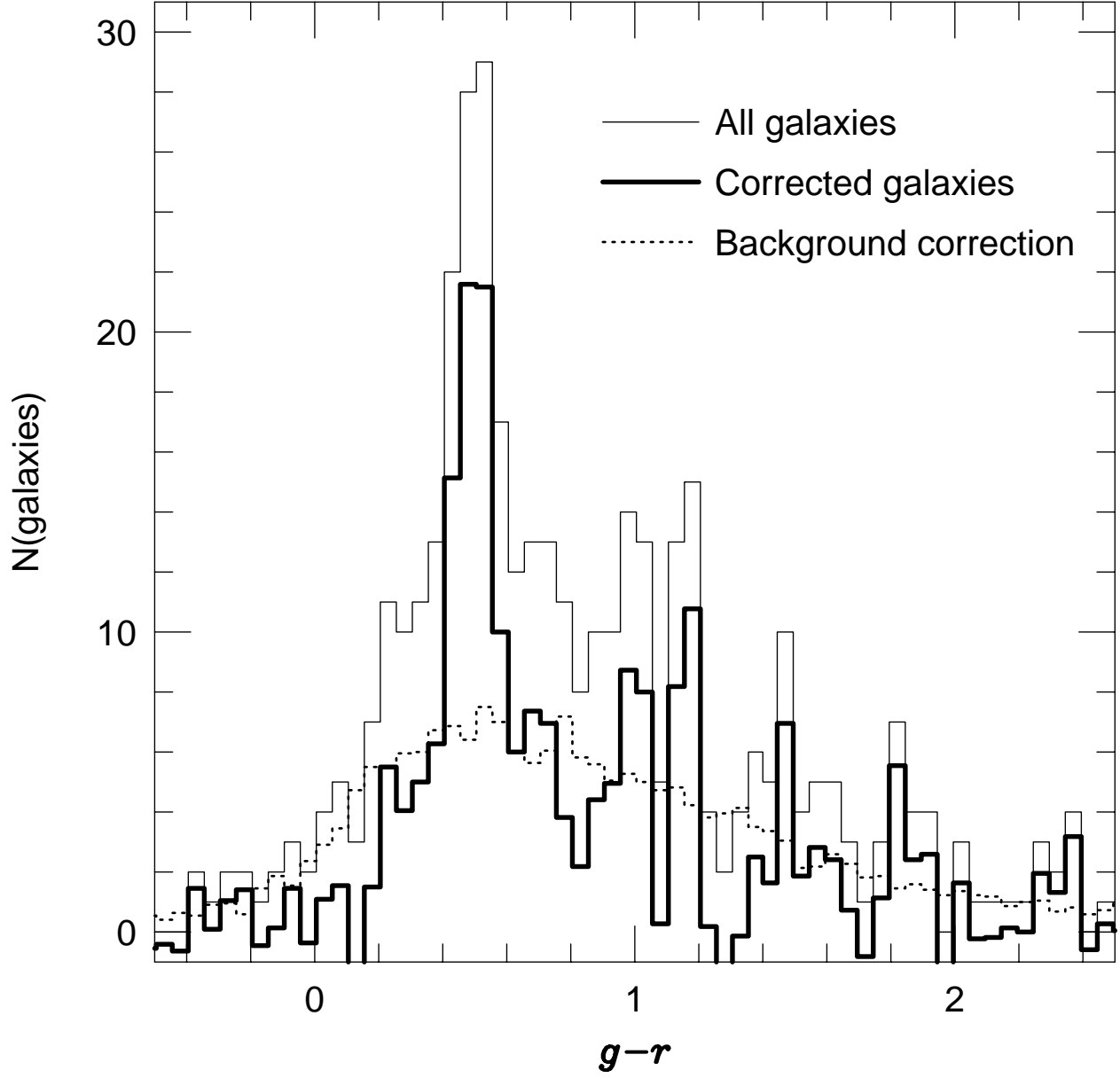


Fig. 2.— An example of the background correction procedure. The thin solid line is the distribution of all galaxy colors ( $g - r$ ) in CCD13 images of Abell 2063. The dotted line is the distribution of galaxy colors derived from our random field observations, while the thick solid line is the background-corrected distribution. A sharp peak at  $(g - r) \sim 0.5$  is seen, corresponding to the early-type galaxy population in this cluster.

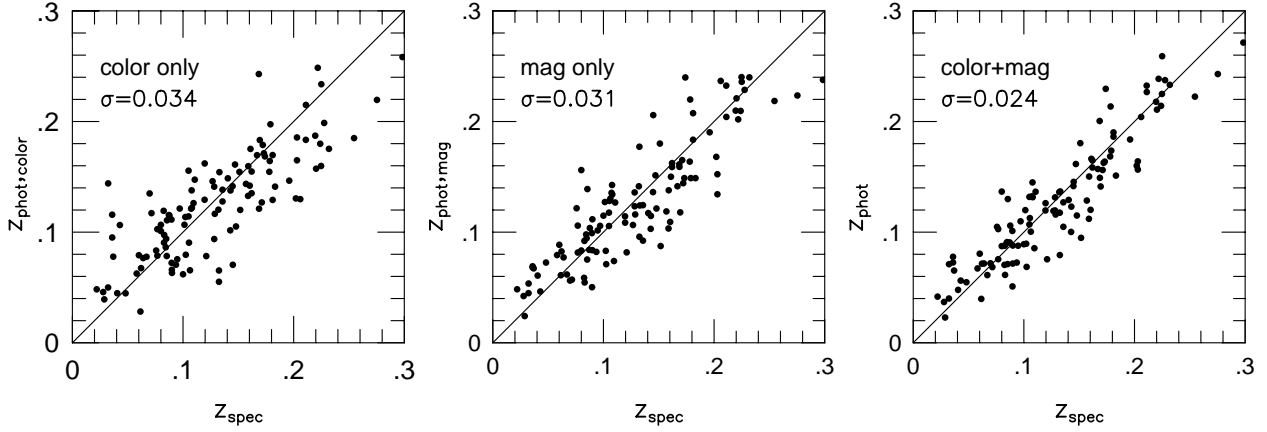


Fig. 3.— The photometric redshift estimates for the CCD13 data plotted against the spectroscopic redshifts, using magnitudes only, colors only, and the combination of colors and magnitudes to derive the estimates. The decrease in scatter is clearly seen.

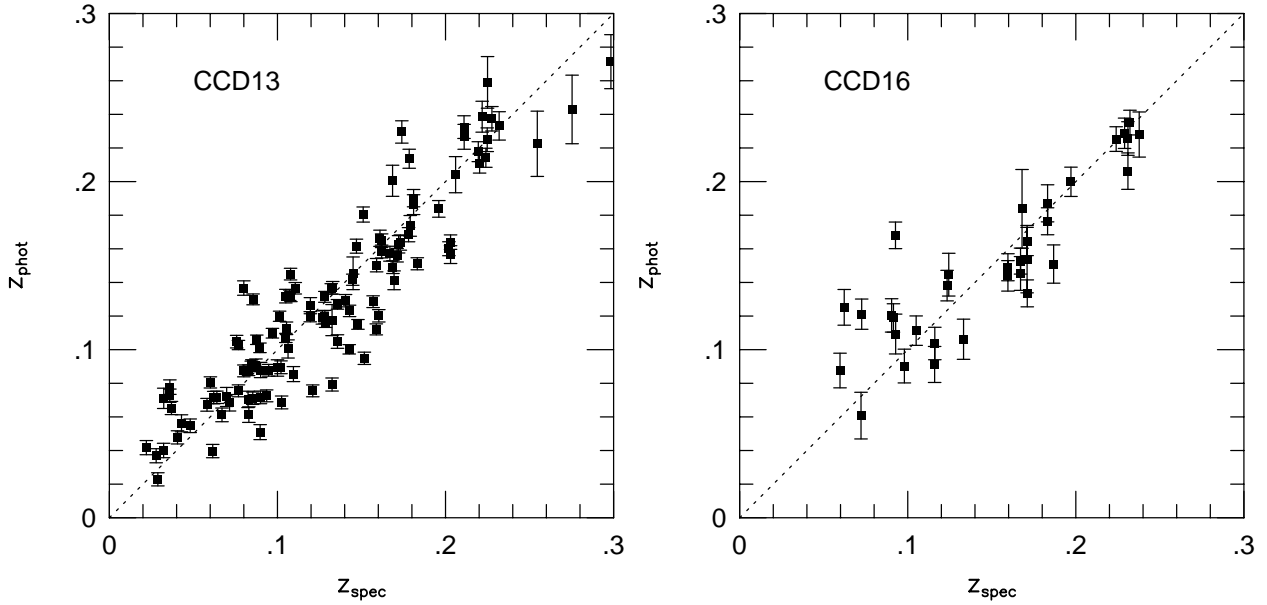


Fig. 4.— The photometrically estimated redshift against the spectroscopically measured redshift for both CCDs. Error bars on individual redshifts represent the one-sigma redshift limits from the bootstrap procedure. The 114 clusters used to derive the relation for CCD13 are on the left, while the 33 clusters used for CCD16 are on the right.

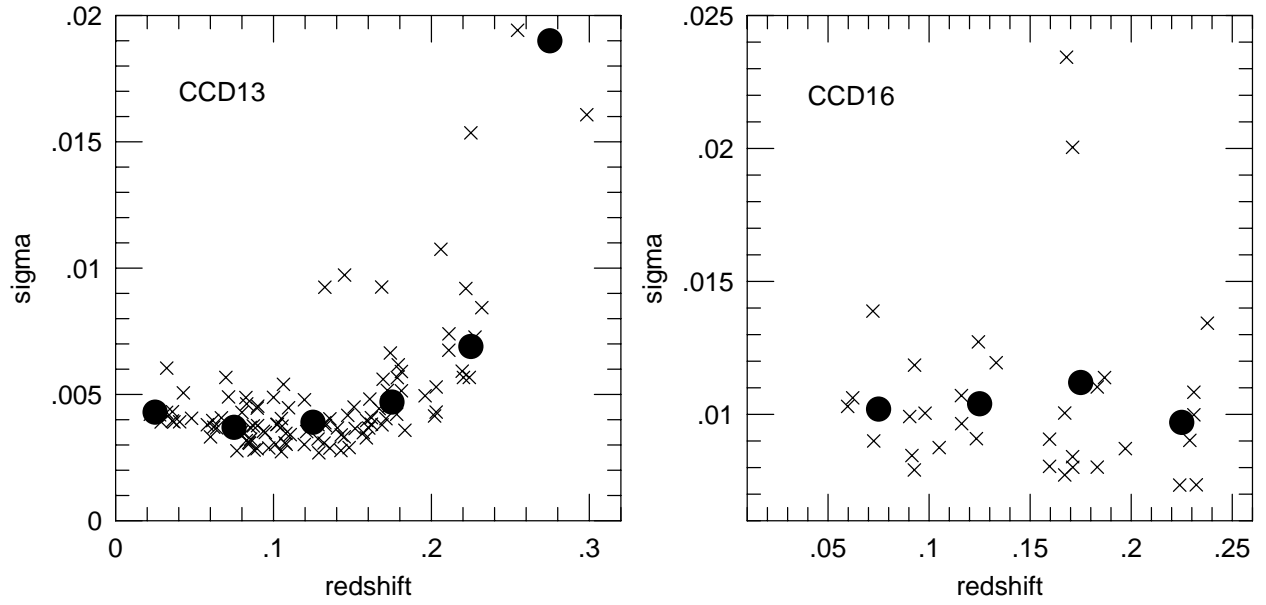


Fig. 5.— Crosses show the error of each cluster redshift, as determined by our bootstrap simulation. Solid circles show the mean redshift errors in redshift bins of  $\Delta z = 0.05$ . The left panel shows the 114 clusters from CCD13, while the right panel shows the 33 clusters from CCD16.

Table 3. Cluster Properties & Photometric Redshifts

Abell	CCD	$(g-r)_{med}$	$g_{mean}$	$E(B-V)$	$z_{phot}$	Error	$z_{spec}$
21	13	0.56984	19.1749	0.03911	0.0881	0.0243	0.0946
26	13	0.68976	19.8172	0.06752	0.1448	0.0243	0.1449
31	16	0.62472	19.9006	0.03836	0.1452	0.0289	0.1596
31	16	0.65092	19.7028	0.03686	0.1498	0.0289	0.1596
54	13	0.75757	20.4157	0.04703	0.1947	0.0245	-
59	13	0.71243	20.1403	0.05342	0.1660	0.0245	-
60	13	0.97409	19.9467	0.04778	0.2061	0.0250	-
62	16	0.50123	19.4658	0.03938	0.0933	0.0289	-
65	16	0.78512	20.0763	0.06377	0.2026	0.0287	0.1206 <sup>a</sup>
68	13	1.11481	20.5031	0.09476	0.2233	0.0250	0.2546
69	13	0.64688	20.1062	0.05788	0.1415	0.0243	0.1454
69	16	0.84825	19.2846	0.05788	0.1899	0.0292	0.1454
73	13	1.05318	20.3368	0.09367	0.2244	0.0250	-
79	16	0.69633	19.7945	0.08488	0.1676	0.0292	0.0927 <sup>a</sup>
82	13	0.64521	19.4615	0.03514	0.1181	0.0243	-
83	16	0.80527	20.2038	0.08388	0.2119	0.0287	-
98	13	0.57916	19.7885	0.04508	0.1073	0.0243	0.1050
98	16	0.58635	19.0310	0.04508	0.1136	0.0289	0.1050
110	13	0.49108	19.4000	0.04784	0.0715	0.0243	-
115	16	0.90548	19.3913	0.05764	0.1995	0.0292	0.1971
136	16	0.90075	20.5781	0.05666	0.2418	0.0287	0.1569
137	16	0.58929	19.6325	0.06651	0.1264	0.0289	-
142	16	1.19339	20.3110	0.02611	0.1846	0.0292	-
143	16	0.64219	20.2976	0.07644	0.1617	0.0292	-
152	13	0.51463	18.8969	0.03561	0.0679	0.0243	0.0581
153	13	0.61917	20.1015	0.03076	0.1313	0.0243	0.1279
153	13	0.64632	19.4959	0.03076	0.1196	0.0243	0.1279
154	13	0.50904	19.1955	0.06283	0.0722	0.0243	0.0624
163	16	0.62553	20.2190	0.05280	0.1532	0.0292	-
165	13	0.60361	19.7734	0.05807	0.1149	0.0243	-
167	16	0.68404	20.3669	0.05187	0.1795	0.0292	-
175	13	0.47655	18.6362	0.05604	0.0549	0.0243	0.1292
175	13	0.60273	19.8184	0.05604	0.1160	0.0243	0.1292
184	13	0.90874	20.8581	0.03488	0.2598	0.0306	-
184	16	0.82114	20.6201	0.03484	0.2306	0.0287	-
191	13	0.90729	20.6865	0.06023	0.2477	0.0250	-
196	13	0.91350	20.1011	0.07062	0.2117	0.0250	-
219	13	0.70417	18.9628	0.07354	0.1182	0.0243	-
227	13	0.67306	20.0422	0.07266	0.1482	0.0243	0.1768
234	13	0.67408	20.3887	0.06394	0.1634	0.0245	0.1731
245	13	0.47259	19.1110	0.05571	0.0616	0.0243	0.0790 <sup>b</sup>
246	13	0.53622	18.6123	0.06930	0.0677	0.0243	0.0700 <sup>b</sup>
247	16	0.70622	19.9252	0.05394	0.1745	0.0292	-
249	13	0.69410	20.6258	0.07400	0.1824	0.0245	-
249	13	0.85473	20.4095	0.07359	0.2208	0.0250	-
253	13	1.05273	19.1403	0.09358	0.1617	0.0245	-
257	16	0.61246	19.6717	0.05504	0.1355	0.0289	0.0703
258	13	0.09506	18.7597	0.10749	0.0111	0.0244	-
258	13	0.15118	18.8687	0.10749	0.0075	0.0244	-
260	13	0.48142	19.2192	0.04944	0.0656	0.0243	0.0369
262	13	0.52546	18.2927	0.09019	0.0598	0.0243	0.0163
272	13	0.57489	19.7996	0.04788	0.1062	0.0243	0.0877
275	16	0.86527	20.2964	0.05229	0.2268	0.0287	-
278	13	0.56409	19.7509	0.05465	0.1013	0.0243	0.0891
288	13	0.70207	19.6760	0.06845	0.1430	0.0243	-
288	13	0.71702	19.5644	0.06845	0.1431	0.0243	-
300	16	0.72066	20.2539	0.05813	0.1890	0.0292	-
307	13	1.94115	19.4678	0.09527	0.0051	0.0244	-
311	13	0.49321	18.2959	0.16897	0.0533	0.0243	0.0649 <sup>b</sup>
318	13	0.65820	19.8653	0.06498	0.1363	0.0243	0.1320
320	13	0.91160	20.1860	0.08404	0.2165	0.0250	-
330	13	0.58288	20.2481	0.09242	0.1231	0.0243	-
333	16	0.70736	19.9606	0.09204	0.1759	0.0292	-
345	13	0.61722	19.2636	0.16864	0.1038	0.0243	-
347	13	1.09518	17.3148	0.05747	0.0950	0.0243	0.0184

Table 3—Continued

Abell	CCD	$(g - r)_{med}$	$g_{mean}$	$E(B - V)$	$z_{phot}$	Error	$z_{spec}$
349	13	0.57984	19.3553	0.06075	0.0955	0.0243	—
360	13	0.85185	20.2633	0.07576	0.2116	0.0250	0.2205
364	13	0.66718	20.1751	0.16586	0.1516	0.0245	0.1800 <sup>b</sup>
372	13	0.64544	19.8768	0.09561	0.1324	0.0243	0.1073
373	13	0.63530	19.4034	0.15390	0.1486	0.0243	—
373	13	0.66272	20.1405	0.15390	0.1133	0.0243	—
374	13	0.61523	19.3218	0.05121	0.1049	0.0243	0.0757
376	13	0.49633	18.3979	0.07008	0.0554	0.0243	0.0481
377	13	0.74239	19.7053	0.14500	0.1937	0.0245	—
377	13	0.75779	20.3970	0.14423	0.1560	0.0245	—
382	13	0.57552	19.7137	0.05816	0.1040	0.0243	—
384	16	0.97386	20.3809	0.04618	0.2356	0.0287	—
397	13	0.40766	18.5634	0.15054	0.0405	0.0244	0.0327
399	13	0.45026	19.8261	0.16449	0.0686	0.0243	0.0724
408	13	0.65978	19.6092	0.22645	0.1275	0.0243	—
410	13	0.42726	19.1095	0.10081	0.0512	0.0243	0.0897
411	16	0.51087	19.3963	0.08243	0.0953	0.0289	0.1567 <sup>b</sup>
421	13	0.50475	18.5584	0.36592	0.0597	0.0243	—
421	13	0.57261	19.1531	0.34166	0.0884	0.0243	—
426	16	0.60447	19.4184	0.17631	0.1273	0.0289	0.0179
427	13	0.69380	19.5394	0.19721	0.1354	0.0243	—
429	13	0.66930	19.2705	0.36639	0.1189	0.0243	—
429	13	0.72971	18.8353	0.36639	0.1201	0.0243	—
436	13	0.52151	18.4605	0.27183	0.0617	0.0243	—
437	13	0.55318	19.4990	0.04673	0.0913	0.0243	0.0847
439	13	0.63436	18.9645	0.18273	0.1002	0.0243	0.1068
444	13	0.56523	19.1289	0.15907	0.0858	0.0243	—
452	13	0.74202	20.1905	0.17141	0.1781	0.0245	—
461	13	0.94078	19.9688	0.09804	0.2063	0.0250	—
465	13	0.65280	19.7421	0.26737	0.1300	0.0243	0.1300 <sup>b</sup>
468	13	0.55633	18.9604	0.18108	0.0796	0.0243	0.1325
468	13	0.73595	18.7085	0.18108	0.1174	0.0243	0.1325
477	13	0.92203	20.5368	0.19900	0.2394	0.0250	—
477	13	1.13313	20.2364	0.19900	0.2033	0.0250	—
478	13	0.59300	18.9106	0.50950	0.0880	0.0243	0.0881 <sup>b</sup>
485	13	0.73114	19.6791	0.19952	0.1517	0.0245	—
497	13	0.53389	18.8471	0.33775	0.0716	0.0243	—
498	13	0.54786	18.3495	0.40129	0.0655	0.0243	—
501	13	0.53564	19.8623	0.20177	0.0952	0.0243	0.1517
502	13	0.47876	17.9946	0.16282	0.0465	0.0244	—
504	13	0.53734	19.0054	0.13891	0.0757	0.0243	—
508	13	0.61470	19.6654	0.13706	0.1151	0.0243	0.1479
509	13	0.68490	20.2419	0.14506	0.1609	0.0245	0.0836
515	13	0.44215	18.3532	0.09844	0.0443	0.0244	—
520	13	0.71559	19.9856	0.04703	0.1601	0.0245	0.1990
523	13	0.60029	18.8808	0.14601	0.0891	0.0243	0.1000
525	13	0.67672	19.8333	0.13798	0.1412	0.0243	—
526	13	0.54725	19.4433	0.09844	0.0882	0.0243	0.0835
529	13	0.52781	19.1887	0.08734	0.0770	0.0243	—
530	13	0.71692	18.6154	0.07989	0.1103	0.0243	—
532	13	0.66377	19.3781	0.21411	0.1209	0.0243	—
537	13	0.83142	20.5565	0.13948	0.2244	0.0250	—
539	13	0.31046	18.2052	0.16181	0.0232	0.0244	0.0284
541	13	1.44808	17.8569	0.19176	0.0496	0.0244	—
546	13	0.83132	19.8455	0.19558	0.1847	0.0245	—
549	13	0.99926	20.4647	0.14110	0.2371	0.0250	—
553	13	0.46492	19.2178	0.15635	0.0615	0.0243	0.0664
554	13	0.54244	19.0158	0.10251	0.0772	0.0243	—
556	13	0.65611	18.8411	0.09980	0.1024	0.0243	—
557	13	1.37318	19.9090	0.10900	0.1117	0.0243	—
558	13	0.17091	18.2115	0.10936	0.0846	0.0243	—
558	13	0.57205	19.0006	0.10936	0.0105	0.0244	—
567	13	0.59490	19.8080	0.11074	0.1131	0.0243	—
567	13	0.60708	20.1740	0.11074	0.1295	0.0243	—
569	13	0.61141	19.0390	0.07308	0.0961	0.0243	0.0201

Table 3—Continued

Abell	CCD	$(g - r)_{med}$	$g_{mean}$	$E(B - V)$	$z_{phot}$	Error	$z_{spec}$
574	13	0.96262	20.3645	0.03163	0.2309	0.0250	0.1740
579	16	0.60821	19.5383	0.06854	0.1311	0.0289	–
580	13	0.47746	19.7908	0.07691	0.0756	0.0243	–
583	16	0.66862	20.0568	0.06291	0.1651	0.0292	–
586	16	0.67197	19.9786	0.05758	0.1642	0.0292	0.1710
587	13	0.55457	19.9488	0.06260	0.1038	0.0243	0.1680
590	13	0.53404	20.0988	0.05466	0.1010	0.0243	–
611	13	0.61826	20.3126	0.04781	0.1388	0.0243	0.2880
630	13	0.69993	20.6623	0.04882	0.1865	0.0245	–
635	13	0.46777	19.3110	0.04504	0.0638	0.0243	–
647	13	0.86745	20.5141	0.02353	0.2299	0.0250	–
657	13	0.06363	19.7952	0.02951	0.0080	0.0244	–
657	13	0.59567	19.3910	0.02951	0.1011	0.0243	–
658	13	0.57290	19.8568	0.03135	0.1073	0.0243	0.0917 <sup>b</sup>
659	13	0.62426	19.4196	0.05547	0.1105	0.0243	–
660	13	0.68376	20.5299	0.04733	0.1736	0.0245	–
665	13	0.36927	19.8699	0.04360	0.0487	0.0244	0.1819
668	13	0.55004	19.6021	0.05564	0.1621	0.0245	0.1588 <sup>b</sup>
677	13	0.70330	21.1855	0.04541	0.2430	0.0250	–
677	13	1.10518	20.7766	0.04360	0.2168	0.0250	–
687	13	0.94758	20.5253	0.02483	0.2407	0.0250	–
688	13	0.66148	19.9358	0.02399	0.1401	0.0243	–
696	13	0.66665	20.2914	0.02464	0.1563	0.0245	–
699	13	0.50383	19.2307	0.05015	0.0716	0.0243	0.0851
706	13	0.68127	20.7678	0.05126	0.1843	0.0245	–
710	13	0.82540	20.8878	0.03391	0.2441	0.0250	–
715	13	0.70071	20.9068	0.03819	0.1998	0.0245	0.1685
720	13	1.03609	20.8913	0.03034	0.2635	0.0306	0.1329 <sup>a</sup>
2 724	16	0.53159	18.5909	0.02975	0.0895	0.0289	0.0933 <sup>b</sup>
732	13	0.64268	20.5079	0.04848	0.1637	0.0245	0.2030
732	13	0.68154	20.3330	0.04848	0.1563	0.0245	0.2030
734	13	0.81491	20.6592	0.03223	0.2264	0.0250	0.0719
741	16	0.87969	19.7788	0.02001	0.2102	0.0287	–
749	13	0.69543	20.0636	0.04477	0.1568	0.0245	–
750	13	0.69561	20.2390	0.04248	0.1583	0.0245	0.1800
750	13	0.70324	20.0379	0.04248	0.1646	0.0245	0.1800
752	13	0.63009	20.6341	0.02153	0.1565	0.0245	–
752	13	0.91807	20.1178	0.02630	0.2131	0.0250	–
759	16	0.94435	20.0263	0.01980	0.2228	0.0287	–
779	13	0.95300	20.9636	0.01599	0.2717	0.0306	0.0229 <sup>a</sup>
781	13	1.02474	20.9976	0.02206	0.2725	0.0306	0.2980
791	13	0.79105	20.1921	0.03118	0.1929	0.0245	–
795	13	0.54773	20.0723	0.02871	0.1050	0.0243	0.1359
795	13	0.62135	19.9541	0.02962	0.1269	0.0243	0.1359
815	13	0.90653	20.5706	0.01982	0.2399	0.0250	–
835	13	0.62725	20.1492	0.03356	0.1360	0.0243	–
850	13	0.61231	20.1526	0.03610	0.1307	0.0243	–
851	16	1.26743	20.9694	0.01711	0.1746	0.0292	0.4069
891	13	0.75560	20.4164	0.01970	0.1940	0.0245	–
898	16	0.90464	20.6850	0.01030	0.2464	0.0287	–
937	13	0.56146	19.9056	0.04112	0.1048	0.0243	–
942	13	0.58843	20.1755	0.01418	0.1227	0.0243	–
954	16	0.59112	19.3193	0.03458	0.1207	0.0289	0.0932
957	16	0.87561	19.4017	0.03351	0.1971	0.0292	0.0450 <sup>a</sup>
2 967	16	0.84000	20.1400	0.01359	0.2169	0.0287	–
969	16	0.50442	18.8411	0.03372	0.0852	0.0289	–
986	13	0.85127	20.6757	0.04148	0.2368	0.0250	–
1015	13	1.29165	20.5934	0.01384	0.1684	0.0245	–
1019	16	0.72710	20.3242	0.01938	0.1934	0.0292	–
1030	16	0.85723	20.3117	0.01841	0.2261	0.0287	0.1780 <sup>b</sup>
1034	13	0.72808	20.0985	0.03329	0.1692	0.0245	–
1050	16	0.58565	19.3148	0.01948	0.1188	0.0289	0.1208 <sup>b</sup>
1062	13	0.76750	20.5136	0.03201	0.2033	0.0250	–
1063	13	0.68803	20.2837	0.04027	0.1639	0.0245	–
1081	13	0.57394	20.0114	0.01671	0.1123	0.0243	0.1585



Table 3—Continued

Abell	CCD	$(g - r)_{med}$	$g_{mean}$	$E(B - V)$	$z_{phot}$	Error	$z_{spec}$
1095	13	0.69758	20.4506	0.02989	0.1752	0.0245	0.2108 <sup>b</sup>
1095	13	0.73707	20.2775	0.02989	0.1808	0.0245	0.2108 <sup>b</sup>
1101	16	0.92782	20.3118	0.01740	0.2331	0.0287	0.2322
1114	13	0.47207	20.1248	0.02872	0.0811	0.0243	0.0140
1120	13	0.79550	20.9401	0.02972	0.2383	0.0250	0.2218
1140	13	1.17952	20.9944	0.01990	0.2347	0.0250	—
1299	13	0.41872	20.1729	0.02565	0.0661	0.0243	0.2247
1345	13	0.50007	19.9364	0.04435	0.0856	0.0243	0.1095
1356	13	0.44753	20.0358	0.04992	0.0718	0.0243	0.0698
1413	13	0.57322	19.6151	0.02308	0.1005	0.0243	0.1427
1441	13	0.56523	19.5451	0.01963	0.0961	0.0243	—
1445	13	0.60697	20.4888	0.02511	0.1411	0.0243	0.1694
1475	13	0.71660	20.7940	0.03053	0.2002	0.0250	—
1481	13	0.46412	20.1934	0.03169	0.0801	0.0243	—
1487	13	0.80138	20.7258	0.01770	0.2265	0.0250	0.2111
1489	13	1.03265	19.9782	0.02366	0.2055	0.0250	0.2060
1495	13	0.59984	20.0652	0.02300	0.1231	0.0243	0.1429
1497	13	0.65830	20.3739	0.02513	0.1567	0.0245	0.1669
1499	13	0.60883	20.1277	0.03933	0.1285	0.0243	0.1569
1526	13	0.52537	19.6862	0.04942	0.0875	0.0243	0.0800
1551	16	0.70359	19.6431	0.01295	0.1658	0.0292	—
1577	13	0.59981	19.8800	0.02463	0.1170	0.0243	0.1409 <sup>b</sup>
1578	16	0.63441	19.1858	0.02452	0.1323	0.0289	—
1592	16	0.86737	20.3286	0.01626	0.2283	0.0287	—
1608	16	0.73723	19.3522	0.01494	0.1678	0.0292	0.1319 <sup>b</sup>
1613	16	0.67606	19.7880	0.01833	0.1606	0.0292	0.1608 <sup>b</sup>
1620	13	0.45548	19.8524	0.02533	0.0705	0.0243	0.0821
1647	16	0.78172	19.9377	0.02458	0.1972	0.0292	—
1656	13	0.42058	18.5126	0.00840	0.0423	0.0244	0.0231
1657	16	0.77811	19.6795	0.02757	0.1881	0.0292	—
1661	16	0.66630	19.6312	0.01671	0.1532	0.0292	0.1690
1661	16	0.68407	19.1141	0.01671	0.1463	0.0289	0.1690
1670	16	1.19250	19.5283	0.02222	0.1627	0.0292	—
1677	16	0.87111	19.1111	0.00942	0.1875	0.0292	0.1820
1680	13	0.48350	19.8260	0.01743	0.0781	0.0243	—
1694	16	0.82213	19.9190	0.01146	0.2058	0.0287	—
1711	13	0.46982	19.7342	0.02744	0.0723	0.0243	—
1712	16	1.01113	20.7184	0.01231	0.2457	0.0287	—
1714	16	0.96882	20.6158	0.01342	0.2242	0.0287	—
1714	16	1.09522	20.5804	0.01342	0.2450	0.0287	—
1717	13	0.64266	20.0143	0.01437	0.1365	0.0243	—
1719	13	1.01227	19.7564	0.00958	0.1947	0.0245	—
1728	13	0.44244	18.8809	0.02792	0.0513	0.0243	—
1739	16	0.56328	19.5497	0.01693	0.1157	0.0289	—
1746	13	0.74077	20.3378	0.00950	0.1850	0.0245	—
1752	13	0.53579	20.5101	0.01115	0.1137	0.0243	—
1759	16	1.09547	19.6304	0.02935	0.1919	0.0292	0.1680
1760	16	0.61888	19.5574	0.02926	0.1352	0.0289	0.1711
1785	13	0.60443	20.1930	0.01169	0.1292	0.0243	0.2136
1795	16	0.57284	19.9279	0.01240	0.1266	0.0289	0.0631
1799	13	0.91528	20.7716	0.01594	0.2546	0.0306	0.2451
1810	16	0.68330	19.5209	0.01207	0.1561	0.0292	—
1813	16	0.54633	19.0667	0.01668	0.1015	0.0289	0.0947 <sup>b</sup>
1820	13	0.81117	20.6951	0.02743	0.2275	0.0250	—
1821	16	0.61573	19.3145	0.01523	0.1289	0.0289	—
1826	16	0.86756	19.8284	0.01636	0.2104	0.0287	—
1856	13	0.56361	20.5709	0.01695	0.1267	0.0243	0.1854 <sup>b</sup>
1874	16	0.73527	19.2227	0.01704	0.1638	0.0292	—
1889	16	0.43053	19.5939	0.01446	0.0730	0.0289	0.1860 <sup>b</sup>
1900	16	0.73368	19.3106	0.01198	0.1657	0.0292	0.1718 <sup>b</sup>
1905	13	0.90926	20.5457	0.01967	0.2386	0.0250	0.3392 <sup>b</sup>
1909	13	0.26985	18.7493	0.02100	0.0217	0.0244	0.1456 <sup>a</sup>
1914	13	0.70911	19.9440	0.02253	0.1562	0.0245	0.1712
1917	13	0.65653	20.7987	0.03411	0.1753	0.0245	—
1926	13	0.45225	19.0446	0.03235	0.0558	0.0243	0.1338

Table 3—Continued

Abell	CCD	$(g - r)_{med}$	$g_{mean}$	$E(B - V)$	$z_{phot}$	Error	$z_{spec}$
1934	13	0.81717	20.5205	0.01296	0.2185	0.0250	0.2194
1954	13	0.49161	20.5259	0.01765	0.0976	0.0243	0.1810
1965	16	1.33724	20.8859	0.01321	0.1213	0.0289	—
1965	16	1.39209	21.0136	0.01321	0.1420	0.0289	—
1965	16	1.52184	20.8693	0.01321	0.0707	0.0289	—
1979	13	0.69590	19.8762	0.01644	0.1491	0.0243	0.1687
1987	16	0.60901	19.0374	0.01949	0.1210	0.0289	—
1990	13	0.83691	20.4901	0.02416	0.2217	0.0250	0.1269
2005	16	0.65914	19.1451	0.02643	0.1393	0.0289	0.1234
2008	13	0.75044	20.3750	0.05147	0.1902	0.0245	0.1810
2016	13	0.65029	20.2297	0.04019	0.1477	0.0243	—
2017	13	0.62659	20.1667	0.04933	0.1364	0.0243	0.1187
2034	16	0.68979	18.7973	0.01520	0.1405	0.0289	0.1130 <sup>b</sup>
2042	16	0.59510	19.7934	0.01658	0.1319	0.0289	0.2353 <sup>a</sup>
2063	13	0.66303	19.9529	0.03458	0.1412	0.0243	0.0353 <sup>a</sup>
2065	16	0.39157	19.3454	0.04122	0.0595	0.0289	0.0726
2069	16	0.50431	19.3059	0.02346	0.0918	0.0289	0.1160
2110	16	0.51463	19.0823	0.02508	0.0917	0.0289	0.0980
2111	16	0.97285	20.2236	0.02595	0.2296	0.0287	0.2290
2116	13	1.29418	20.4549	0.03000	0.1611	0.0245	—
2126	13	0.71284	20.4204	0.06225	0.1793	0.0245	0.1656 <sup>b</sup>
2129	13	0.74726	20.3378	0.05130	0.1872	0.0245	—
2141	16	0.60366	20.0573	0.02138	0.1410	0.0289	0.1584 <sup>b</sup>
2141	16	0.79995	19.6468	0.02125	0.1923	0.0292	0.1584 <sup>b</sup>
2147	13	0.48392	19.8084	0.03332	0.0727	0.0243	0.0350
2147	13	0.48680	19.5180	0.03332	0.0779	0.0243	0.0350
2152	13	0.41326	19.6833	0.04018	0.0565	0.0243	0.0410
2155	13	1.17570	20.4862	0.06581	0.2054	0.0250	0.2465 <sup>b</sup>
2157	13	1.02867	21.0270	0.01809	0.2743	0.0306	—
2160	16	0.80138	20.2053	0.03127	0.2110	0.0287	—
2162	13	0.43867	20.1324	0.03728	0.0711	0.0243	0.0322
2170	13	0.49221	19.2521	0.08171	0.0690	0.0243	0.1030
2173	13	0.61042	20.2919	0.06308	0.1350	0.0243	—
2177	13	0.67667	20.4227	0.03891	0.1659	0.0245	0.1610
2178	16	0.53237	19.8593	0.05602	0.1105	0.0289	0.0928
2188	16	0.47539	20.1565	0.02184	0.0952	0.0289	—
2192	16	0.61924	20.2626	0.01013	0.1519	0.0292	0.1875
2193	13	0.45168	20.0398	0.04102	0.0731	0.0243	—
2195	13	0.86845	20.3751	0.01547	0.2215	0.0250	—
2196	16	0.52552	19.8127	0.00573	0.1072	0.0289	0.1339
2197	13	0.46110	18.2195	0.00777	0.0461	0.0244	0.0308
2198	13	0.90143	20.8216	0.00694	0.2562	0.0306	0.0798
2199	13	0.61377	19.3977	0.01070	0.1067	0.0243	0.0299
2199	16	0.56860	19.0855	0.01070	0.1089	0.0289	0.0299
2200	13	0.70059	20.0345	0.06997	0.1573	0.0245	—
2205	13	0.52694	19.8040	0.05611	0.0909	0.0243	0.0876
2215	13	0.83647	20.6864	0.02702	0.2339	0.0250	—
2217	16	0.67713	19.6565	0.05380	0.1575	0.0292	—
2219	13	0.97399	20.2862	0.02349	0.2262	0.0250	0.2256
2221	13	0.75515	20.2772	0.01248	0.1866	0.0245	0.1019 <sup>b</sup>
2228	13	0.62752	19.6874	0.04829	0.1200	0.0243	0.1013
2229	13	0.75386	20.3148	0.02118	0.1882	0.0245	—
2238	13	0.67963	20.1779	0.01715	0.1562	0.0245	—
2240	13	0.74809	20.7689	0.04179	0.2110	0.0250	0.1380
2241	16	0.51370	19.5172	0.03004	0.0982	0.0289	—
2243	13	0.63968	20.1087	0.02133	0.1390	0.0243	—
2244	13	0.57937	19.8780	0.02313	0.1100	0.0243	0.0968
2246	13	1.03852	20.8495	0.02377	0.2602	0.0306	0.2250
2251	16	0.72084	20.1940	0.04985	0.1873	0.0292	—
2252	13	0.79111	20.6880	0.01414	0.2210	0.0250	0.1147
2254	13	0.70617	20.2366	0.05330	0.1682	0.0245	0.1780
2255	13	0.68960	19.6058	0.02622	0.1366	0.0243	0.0806
2256	13	0.53847	19.2448	0.04982	0.0811	0.0243	0.0581
2257	13	0.62971	19.4428	0.04085	0.1128	0.0243	0.1054
2261	16	0.56827	20.2002	0.04453	0.1306	0.0289	0.2240 <sup>b</sup>

Table 3—Continued

Abell	CCD	$(g - r)_{med}$	$g_{mean}$	$E(B - V)$	$z_{phot}$	Error	$z_{spec}$
2262	13	0.91988	20.5466	0.05507	0.2399	0.0250	–
2262	16	0.89261	20.1596	0.05507	0.2251	0.0287	–
2263	13	0.60642	20.2462	0.04994	0.1319	0.0243	0.1051
2266	16	0.71157	20.3038	0.04183	0.1875	0.0292	0.1671
2267	13	0.86400	20.5473	0.02297	0.2313	0.0250	–
2268	13	0.73229	20.4696	0.03480	0.1888	0.0245	–
2269	13	1.16571	21.0218	0.03386	0.2415	0.0250	–
2270	16	0.78089	20.7234	0.03440	0.2240	0.0287	0.2377
2272	13	0.62073	20.2334	0.05035	0.1368	0.0243	0.1329
2273	13	1.01048	20.7064	0.03138	0.2527	0.0306	–
2274	13	1.02068	19.8009	0.03767	0.1966	0.0245	–
2275	13	0.52463	19.7815	0.04312	0.0896	0.0243	0.1029
2278	13	0.73838	20.6429	0.03667	0.2003	0.0250	–
2279	13	0.65266	19.8254	0.07495	0.1330	0.0243	–
2285	16	0.43095	19.1077	0.02784	0.0675	0.0289	–
2286	13	0.53359	19.6268	0.04234	0.0886	0.0243	–
2288	13	0.48939	19.3434	0.06314	0.0700	0.0243	–
2289	13	0.88125	20.6091	0.04916	0.2385	0.0250	0.2276
2291	13	0.81070	19.9702	0.05685	0.1864	0.0245	0.1810
2292	13	0.64847	18.9927	0.04306	0.1047	0.0243	0.1190 <sup>b</sup>
2297	13	0.50607	20.0410	0.03817	0.0901	0.0243	–
2297	13	0.74219	20.3259	0.04254	0.1849	0.0245	–
2298	13	0.80612	20.0823	0.05148	0.1911	0.0245	–
2299	13	0.55541	20.0556	0.03908	0.1515	0.0245	–
2299	13	0.69345	19.9546	0.05563	0.1071	0.0243	–
2300	13	0.64421	19.5768	0.07032	0.1216	0.0243	–
2310	13	0.63194	19.3633	0.07897	0.1111	0.0243	–
2311	13	0.52620	18.9747	0.06498	0.0722	0.0243	0.0890
2314	13	0.86960	20.0638	0.07862	0.2035	0.0250	–
2315	13	0.52220	19.0739	0.08541	0.0732	0.0243	0.0894
2316	13	0.99357	20.4234	0.09037	0.2346	0.0250	0.2147
2317	13	0.89940	20.4905	0.06625	0.2337	0.0250	0.2110
2318	13	0.60557	20.1790	0.06819	0.1291	0.0243	0.1405
2319	13	0.54066	19.3494	0.11363	0.0841	0.0243	0.0557 <sup>b</sup>
2320	13	0.62367	19.0166	0.17918	0.0988	0.0243	0.1710
2321	13	0.66613	20.2440	0.16135	0.1541	0.0245	–
2322	13	0.69446	19.7792	0.25078	0.1447	0.0243	–
2323	13	0.66152	19.7576	0.09939	0.1334	0.0243	–
2326	13	0.65102	19.4072	0.48845	0.1181	0.0243	–
2327	13	0.61473	19.8558	0.08081	0.1213	0.0243	–
2349	16	0.38086	19.0358	0.04782	0.0540	0.0289	–
2349	16	0.58182	20.0422	0.04858	0.1324	0.0289	–
2353	13	0.52112	19.2298	0.05477	0.0761	0.0243	0.1210
2355	13	1.04350	20.6513	0.06633	0.2458	0.0250	0.1244
2355	16	0.59421	20.4228	0.06633	0.1459	0.0289	0.1244
2356	16	0.54219	19.3538	0.06931	0.1050	0.0289	0.1161
2359	13	0.73060	20.3196	0.08706	0.1807	0.0245	–
2373	13	0.80311	20.8274	0.05509	0.2335	0.0250	–
2379	13	0.68978	19.8457	0.11891	0.1459	0.0243	–
2381	13	0.83569	20.2282	0.05782	0.2061	0.0250	0.0726 <sup>a</sup>
2386	13	0.56365	19.9434	0.07340	0.1067	0.0243	–
2386	13	0.73147	20.4833	0.06705	0.1893	0.0245	–
2387	13	0.80581	19.0725	0.14370	0.1449	0.0243	0.1450
2388	13	0.46280	17.7167	0.05006	0.0405	0.0244	0.0615
2390	16	0.74397	20.4617	0.11311	0.2034	0.0287	0.2280
2390	16	0.81282	20.4291	0.11562	0.2216	0.0287	0.2280
2392	16	0.83911	20.1990	0.07231	0.2189	0.0287	–
2395	13	0.72047	20.0539	0.04946	0.1647	0.0245	0.1508 <sup>b</sup>
2396	13	0.56837	19.7775	0.07442	0.1035	0.0243	0.1946
2397	13	0.81644	20.4615	0.05322	0.2149	0.0250	0.2240
2397	16	0.91703	20.0800	0.05322	0.2240	0.0287	0.2240
2406	16	0.79625	20.4579	0.06294	0.2186	0.0287	–
2407	13	0.62568	19.5082	0.05697	0.1136	0.0243	–
2407	13	0.65888	19.8073	0.05697	0.1344	0.0243	–
2408	13	0.72784	20.4625	0.05279	0.1869	0.0245	–

Table 3—Continued

Abell	CCD	$(g - r)_{med}$	$g_{mean}$	$E(B - V)$	$z_{phot}$	Error	$z_{spec}$
2409	13	0.67936	20.2982	0.10835	0.1613	0.0245	0.1479
2413	13	0.64357	20.3016	0.08163	0.1480	0.0243	–
2414	13	0.54429	19.6266	0.05859	0.1143	0.0243	–
2414	13	0.66671	19.1478	0.05859	0.0918	0.0243	–
2419	13	0.65240	20.2949	0.05203	0.1511	0.0245	0.0456
2422	16	0.98668	20.5918	0.12078	0.2430	0.0287	–
2423	16	0.53334	19.5092	0.08588	0.1046	0.0289	–
2424	13	0.74243	20.2355	0.06700	0.1804	0.0245	0.1510
2425	13	0.81797	20.7676	0.09094	0.2341	0.0250	–
2425	16	1.13616	20.2419	0.09307	0.2011	0.0287	–
2429	16	0.78587	20.3804	0.06104	0.2131	0.0287	–
2429	16	1.10455	20.6698	0.06104	0.2250	0.0287	–
2431	16	0.63601	20.2324	0.06324	0.1576	0.0292	–
2431	16	0.70041	20.0241	0.06324	0.1754	0.0292	–
2432	13	0.68740	20.2438	0.09827	0.1619	0.0245	–
2435	16	0.73958	20.1356	0.06413	0.1915	0.0292	–
2437	13	0.69214	20.2262	0.08662	0.1628	0.0245	–
2439	16	0.70738	20.2025	0.06611	0.1830	0.0292	–
2440	16	0.57093	19.7181	0.08757	0.1216	0.0289	0.0906
2443	13	0.64240	19.8860	0.06173	0.1317	0.0243	0.1080
2445	13	0.64582	20.3701	0.05318	0.1517	0.0245	–
2447	13	0.44196	19.2650	0.09851	0.0568	0.0243	–
2447	13	0.62960	20.3519	0.09851	0.1447	0.0243	–
2449	13	0.49500	19.6080	0.05987	0.1072	0.0243	–
2449	13	0.58114	19.7637	0.05987	0.0768	0.0243	–
2454	13	0.65046	20.2845	0.13473	0.1500	0.0243	0.1590
2454	16	0.61853	19.8051	0.13443	0.1407	0.0289	0.1590
2454	16	0.65777	19.9817	0.13443	0.1592	0.0292	0.1590
2457	16	0.50568	19.0917	0.08380	0.0891	0.0289	0.0597
2458	16	0.55545	19.8929	0.04334	0.1195	0.0289	–
2471	13	0.66070	20.0663	0.10078	0.1449	0.0243	0.1078
2471	16	0.78578	19.8804	0.10078	0.1964	0.0292	0.1078
2472	13	1.08891	21.0285	0.04027	0.2643	0.0306	–
2475	13	0.82174	20.5048	0.11083	0.2188	0.0250	–
2483	16	0.52421	19.9429	0.06316	0.1090	0.0289	–
2491	16	0.69385	20.2091	0.06395	0.1784	0.0292	–
2494	13	0.68420	19.4728	0.11406	0.1301	0.0243	–
2495	13	0.52068	19.2362	0.07727	0.1030	0.0243	0.0775
2495	13	0.57994	19.6307	0.07727	0.0761	0.0243	0.0775
2503	13	0.44194	19.5523	0.06396	0.0615	0.0243	0.0827
2505	13	0.44775	20.4853	0.06581	0.0813	0.0243	–
2506	13	0.65002	20.5516	0.05708	0.1612	0.0245	0.0289
2507	13	0.76623	20.1576	0.09621	0.1840	0.0245	0.1960
2512	13	0.58753	20.1112	0.08314	0.1202	0.0243	0.1603
2513	13	0.74724	20.5557	0.09173	0.1987	0.0245	0.0250
2515	13	0.84587	20.0317	0.07771	0.1974	0.0245	–
2516	13	0.64835	20.2746	0.10313	0.1488	0.0243	0.0793 <sup>a,b</sup>
2516	16	0.64359	20.3556	0.10313	0.1638	0.0292	0.0793 <sup>a,b</sup>
2517	13	0.76274	19.5212	0.11367	0.1537	0.0245	–
2522	13	0.66416	20.4527	0.09737	0.1624	0.0245	0.1562
2530	13	0.56802	19.7513	0.11501	0.1026	0.0243	–
2532	13	0.69960	20.4157	0.08593	0.1742	0.0245	–
2535	13	0.66319	19.5869	0.14319	0.1278	0.0243	–
2545	13	0.76899	19.8956	0.07205	0.1720	0.0245	–
2551	13	0.50094	20.1173	0.07791	0.0903	0.0243	–
2552	16	0.68599	20.2365	0.05088	0.1764	0.0292	0.1330 <sup>b</sup>
2562	13	0.80266	19.7829	0.06523	0.2218	0.0250	–
2562	13	0.90301	20.2926	0.06446	0.1753	0.0245	–
2570	13	0.53636	18.9403	0.04200	0.0741	0.0243	–
2571	16	0.54843	19.5510	0.04538	0.1105	0.0289	0.1084 <sup>b</sup>
2574	16	0.53587	20.3121	0.05075	0.1203	0.0289	–
2582	16	0.60813	19.8203	0.04932	0.1373	0.0289	–
2584	13	0.58608	20.3071	0.11019	0.1263	0.0243	0.1200
2590	16	0.68153	20.2835	0.03588	0.1762	0.0292	0.0790 <sup>a</sup>
2594	13	0.64749	20.4907	0.09116	0.1575	0.0245	–

Table 3—Continued

Abell	CCD	$(g - r)_{med}$	$g_{mean}$	$E(B - V)$	$z_{phot}$	Error	$z_{spec}$
2602	13	0.66981	20.0542	0.07331	0.1476	0.0243	–
2607	13	0.59903	19.9719	0.05932	0.1197	0.0243	0.1201
2610	13	0.69146	20.2495	0.04707	0.1636	0.0245	–
2616	13	0.67396	20.1020	0.06841	0.1510	0.0245	0.1832
2616	16	0.70984	19.9135	0.06841	0.1753	0.0292	0.1832
2617	16	0.68110	20.3109	0.06647	0.1768	0.0292	0.1630 <sup>b</sup>
2620	13	1.14380	20.9492	0.07324	0.2439	0.0250	0.1911
2621	13	0.97878	20.6458	0.06112	0.2496	0.0250	–
2622	13	0.52331	19.0075	0.05718	0.0722	0.0243	0.0621
2623	13	0.84819	20.3273	0.06631	0.2146	0.0250	0.1784
2624	13	0.89365	20.6794	0.07054	0.2452	0.0250	–
2627	13	0.58119	20.1524	0.07086	0.1193	0.0243	0.1255
2631	13	1.09759	20.7569	0.03792	0.2434	0.0250	0.2730
2631	16	0.98491	20.6245	0.03859	0.2445	0.0287	0.2730
2633	16	0.60596	19.7828	0.05176	0.1356	0.0289	–
2639	16	0.74011	19.8492	0.05066	0.1829	0.0292	–
2649	13	0.50078	19.5811	0.07831	0.0779	0.0243	–
2650	13	0.73413	19.3363	0.06955	0.1389	0.0243	–
2657	13	0.46187	18.4020	0.12911	0.0486	0.0244	0.0402
2666	13	0.39746	18.4351	0.03879	0.0374	0.0244	0.0272
2668	16	0.46489	19.5665	0.03653	0.0831	0.0289	–
2668	16	0.57262	19.6900	0.03718	0.1217	0.0289	–
2671	13	0.67403	20.5999	0.05555	0.1731	0.0245	0.1799
2672	13	0.66410	19.2755	0.04222	0.1176	0.0243	0.2412
2675	16	0.58614	19.5086	0.07751	0.1228	0.0289	0.0713
2695	16	0.53040	19.3407	0.03076	0.1008	0.0289	–
2696	13	0.56125	19.3736	0.03027	0.0906	0.0243	0.0844
2698	16	0.64731	19.5626	0.02219	0.1451	0.0289	0.0979
2706	16	0.57138	19.4338	0.08982	0.1163	0.0289	–
2711	13	0.74385	20.1832	0.04961	0.1783	0.0245	–

<sup>a</sup>The photometric redshift estimate differs significantly from the single-galaxy spectroscopic redshift.

<sup>b</sup>This spectroscopic redshift was obtained after the photometric redshift estimate, and was not used in the derivation.